31st Annual International Conference of the IEEE EMBS
Minneapolis, Minnesota, USA, September 2-6, 2009

Accurate Reconstruction of Brain Activity and Functional Connectivity from Noisy MEG Data

Julia P. Owen[1,2], David P. Wipf[1], Hagai T. Attias[3], Kensuke Sekihara[4], and Srikantan S. Nagarajan[1,2]
[1] Biomagnetic Imaging Laboratory, Dept. Radiology and Biomedical Imaging, UCSF San Francisco, CA, USA
[2] Joint Graduate Group in Bioengineering UCSF/UC Berkeley, San Francisco, CA, USA
[3] Golden Metallic, Inc. San Francisco, CA, USA
[4] Dept. of Systems Design and Engineering, Tokyo Metropolitan University, Tokyo, Japan

Abstract— **The synchronous brain activity measured via magnetoencephalography (MEG) arises from current dipoles located throughout the cortex. Estimating the number, location, time-course, and orientation of these dipoles, called sources, remains a challenging task, one that is significantly compounded by the effects of source correlations and interference from spontaneous brain activity and sensor noise. Likewise, assessing the interactions between the individual sources, known as *functional connectivity*, is also confounded by noise and correlations in the sensor recordings. Computational complexity has been an obstacle to computing functional connectivity. This paper demonstrates the application of an empirical Bayesian method to perform source localization with MEG data in order to estimate measures of functional connectivity. We demonstrate that brain source activity inferred from this algorithm is better suited to uncover the interactions between brain areas as compared to other commonly used source localization algorithms.**

I. Introduction

Magnetoencephalography (MEG) non-invasively detects brain activity from direct measurements of the magnetic field with an array of sensors; the observed field is generated by large ensembles of neurons firing synchronously, approximated as compact current sources. Determining the combination of sources that best explains the field recordings is an ill-posed inverse problem because the number of potential sources is much greater than the number of sensors. Determining the spatial distribution, orientation, and time courses of these unknown sources is an open inverse problem.

We have developed a novel empirical Bayesian scheme, presented in [7] and [8], that improves upon existing methods of source reconstruction in terms of reconstruction accuracy, robustness, and efficiency. The algorithm derived from this model, which we call *Champagne*, is designed to estimate the number and location of a small (sparse) set of flexible dipoles that adequately explain the observed sensor data. This method relies on having access to pre- and post-stimulus data, where the pre-stimulus data is thought to contain no stimulus-evoked brain activity. We have shown that Champagne reliably reconstructs a large number of correlated dipoles. The source time-course estimates from Champagne are well suited for functional connectivity analyses.

Functional connectivity can be described as understanding brain function in terms of the way information is transmitted and integrated across brain networks. In the most complete case, one would like to make inferences from a causal linear model that describes the dependencies among activities across all voxels. However, due to the large number of voxels, solving such a model is computationally expensive and virtually impossible with limited, noisy data. Instead, existing techniques for estimating functional connectivity approximate the full problem in various ways, but there is a tradeoff between reducing the complexity and loss of sensitivity. Paradoxically, inferences about connectivity can be made from the correlations between source time-courses, but many common localization algorithms have significant trouble reconstructing correlated brain activity. Consequently, there is a fundamental problem with applying many existing localization methods to functional connectivity estimation.

The solution obtained from Champagne is ideal for use in functional connectivity analyses as it is robust to highly correlated dipoles and it circumvents the issues of computational complexity by vastly pruning the number of active voxels. We present new results from simulated and real MEG data showing Champagne's efficacy in reconstructing brain activity and estimating functional connectivity as compared to standard localization techniques such as generalized minimum current estimation (MCE) [5], minimum variance adaptive beamforming (MVAB) [4], and sLORETA [3].

II. Methods

A. Source Localization: Champagne

The voxels time-courses (x_n) are inferred from the sensor data (y_n) using a novel source-localization algorithm called *Champagne* described in full detail in [7] and [8]. In summary, this method relies on segmenting the data into pre- and post-stimulus periods, learning the statistics of the background activity from the pre-stimulus period, and then applying the statistics of the background activity to the post-stimulus data to uncover the stimulus-evoked activity. The underlying assumption is that the noise and non-stimulus-locked brain activity present in the pre-stimulus period continues into the post-stimulus period, where the stimulus-evoked activity is linearly superimposed. We model the pre- and post-stimulus sensor data as:

$$y_n^{pre} = Bu_n^{pre} + v_n \quad (1)$$

$$y_n^{post} = Fx_n + Bu_n^{post} + v_n \quad (2)$$

978-1-4244-3296-7/09/$25.00 ©2009 IEEE

where the number of sensors is K, the number of voxels is L, the number of inference factors is M, and the total number of time points is N. y_n is the K x 1 measured electromagnetic signal vector at time $n = 1:N$, x_n is the L x 1 voxel activity vector at time $n = 1:N$, u_n^{pre} and u_n^{post} are the M x 1 pre- and post-stimulus interference factors at time $n = 1:N$, and v_n is the K x 1 sensor noise vector at time $n = 1:N$. F is the K x L leadfield matrix and B is the L x M interference mixing matrix. Using a 2-dimensional leadfield results in the interleaving of the leadfield columns for the two directions. Likewise the number of voxel time courses is doubled to represent the two dipolar directions at every voxel. (This method can also be extended to 3 directions for use with EEG data.) The dimensions of F becomes K x $2L$ and the dimensions of x_n becomes $2L$ x 1. Both v_n and B are learned from the pre-stimulus period using Variation Bayesian Factor Analysis (VBFA) [1] and then used in the estimation of x_n and u_n with the post-stimulus data.

The signals x, u, v are assumed to be independent zero-mean Gaussian distributions. While we make assumptions about the prior distributions, we calculated full posteriors (see below) which affords robustness to these assumptions [1]. The precision matrices for the factors u_n and then sensor noise v_n are diagonal, where u_n^j has precision 1 and v_n^i has has precision λ^i The precision matrix ν^j for each x_n^j is a 2x2 matrix that allows for correlation between the two directions of each dipole at every voxel. The entire precision matrix ν is a $2L$ x $2L$ block-diagonal matrix.

The model distributions are:

$$p(y_n|x_n) = \mathcal{N}(y_n|Fx_n + Bu_n, \lambda) \quad (3)$$
$$p(x_n) = \mathcal{N}(x_n|0, \nu) \quad (4)$$
$$p(u_n) = \mathcal{N}(u_n|0, I) \quad (5)$$
$$p(v_n) = \mathcal{N}(v_n|0, \lambda) \quad (6)$$

We can redefine the notation such that: $x'_n = \begin{pmatrix} x_n \\ u_n^{post} \end{pmatrix}$, $F' = (FB)$, and $\nu' = \begin{pmatrix} \nu & 0 \\ 0 & I \end{pmatrix}$.

With this new notation, the estimation problem in the post-stimulus period reduces to:

$$y_n^{post} = F'x'_n + v_n \quad (7)$$
$$p(x'_n) = \mathcal{N}(x'_n|0, \nu') \quad (8)$$

The posterior over x'_n is Gaussian:

$$p(x'_n|y_n) = \mathcal{N}(x'_n|\bar{x'}_n, \Gamma) \quad (9)$$

where

$$\bar{x'}_n = \Gamma^{-1}F'^T\lambda y_n \quad (10)$$
$$\Gamma = F'^T\lambda F' + \nu' \quad (11)$$

The marginal log-likelihood function in this new notation is:

$$\mathcal{L} = \sum_n \log p(y_n|\nu') = \frac{N}{2}\left(log|\nu'| + log|\Gamma| - Q + constant\right) \quad (12)$$

where $Q = \frac{1}{N}\sum_n \bar{x'}_n \bar{x'}_n^T$. We can derive an updates rule for ν' using an Expectation-Maximization (EM) algorithm, $\nu'^{-1} =$ Q, but this algorithm has a slow convergence rate for a large number of voxels. Thus, we have derived a faster algorithm that uses a fixed point method [6]. The update rule for ν' for this method is:

$$\nu'^{-\frac{1}{2}} = S^{-\frac{1}{2}}(S^{\frac{1}{2}}QS^{\frac{1}{2}})^{\frac{1}{2}}S^{-\frac{1}{2}} \quad (13)$$

where $S = \nu'^{\frac{1}{2}}WF'\nu'^{-\frac{1}{2}}$ and $W = \Gamma^{-1}F'^T\lambda$. The source time courses are estimated from 10 are iteratively computed with ν' in the algorithm. The convergence of Champagne is relatively fast compared to the EM algorithm implementation [7] and can be run in approximately ten minutes for 5000 voxels and 300 post-stimulus time points.

B. Functional Connectivity

We chose to employ two pair-wise connectivity metrics: coherence and imaginary coherence and one multivariate method: multivariate autoregression (MVAR). Coherence is a traditional metric of connectivity and is the frequency domain representation of cross-correlation. The coherence is a complex-valued quantity; we looked at both the magnitude of the coherence and the imaginary part of the coherence alone. *Imaginary coherence* is a relatively new metric developed for use with MEG data [2]. It only reflects the coherence that is non-instantaneously mixed. Functional connectivity methods with MEG are subject to spurious correlations arising from instantaneous correlations at the sensors. Coherence and imaginary coherence contain complimentary information. When pairwise metrics are used, we used the coherence measure to reconstruct the correlations and imaginary coherence to determine which correlations are non-instantaneous.

MVAR models the data as linear mixing of current and past values of the data, where the mixing is done with a *mixing matrix* (of size number of sources by number of sources) at every specified time lag. As compared to the pair-wise metrics, MVAR takes into account all the source voxels and models the data with access to all the information. From the coefficients in the mixing matrix, we can infer which nodes in the network are interacting and the time-lag of interaction. While the pair-wise metrics are symmetric, MVAR yields asymmetric results that can be used to uncover causality in the network. MVAR is a more powerful tool as it both quantifies the time scale of interactions and provides directionality. Typically reducing the number of candidate voxel time-courses limits the usage of MVAR in such functional connectivity analyses, but the sparse solution obtained with Champagne makes this computationally intensive method an option.

C. Experimental Methods

Source Localization: We have tested Champagne using simulated data with realistic source configurations. The data time courses were partitioned into a pre-stimulus period where there is only noise and interfering brain activity and a post-stimulus period where there is the same (statistically) noise and interference factors plus source activity of interest. The pre-stimulus activity consisted of the resting-state sensor recordings collected from a human subject and is

presumed to have spontaneous activity (i.e., non-stimulus evoked sources) and sensor noise; this activity was ongoing and continued into the post-stimulus period, where damped-sinusoidal sources were seeded and projected to the sensors through the leadfield. Champagne was tested against three commonly used source localization algorithms: generalized minimum current estimation (MCE), minimum variance adaptive beamforming (MVAB) and sLORETA in 100 simulation runs. We found that Champagne outperformed these other algorithms in terms of localization accuracy and time-course reconstruction at all four signal-to-noise-plus-interefence ratios tested (-5 to 10dB). These results are not shown, but can be found in [7].

We also ran Champagne on four real-world brain data-sets: an auditory evoked field (AEF) data-set, a auditory feedback perturbation task, a self-paced button press task, and a language processing task. In the AEF task, a tone was presented to a control subject 120 times; this data set is notoriously difficult to reconstruct due to the highly correlated dipoles in the right and left auditory cortices. In the auditory feedback perturbation task, the subjects auditory feedback was pitch-shifted while he/she was actively articulating. In the self-paced button press task, the subject was instructed to press a button at his/her own pace. And in the language processing task, the subject was orally presented with a noun and was asked to think of an associated verb.

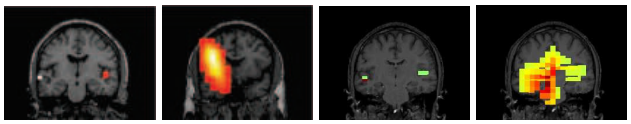

(a)Champagne (b)MVAB (c)Champagne (d)MVAB

Fig. 1. (a) and (b) performance on AEF data. Champagne (a) is able to localize distinct dipoles in left and right auditory cortices. (c) and (d) performance on auditory-feedback data-set showing increased activation in superior temporal gyrus (bilaterally) after the perturbation uncovered with Champagne (c). In both data sets, MVAB (b) and (d) is unable to uncover the correlated auditory activations.

(a)Somato-motor Localization (b)SII Localization

Fig. 2. Champagne is able to uncover activations in motor cortex (bilaterally) and primary somatosensory cortex, SI shown in (a). Champagne is also able to uncover an activation (b) secondary somatosensory cortex, SII, which is generally hard to localize in MEG (shown by cross-hairs)

Functional Connectivity: We used simulated data to investigate Champagne's ability to uncover interacting brain activity. We used Gaussian noise, instead of the real-brain noise described above. We used $SNIR = 5dB$ and an intra-dipole correlation of 0.5. We simulated a network of 7 nodes (or voxels), where there were two networks, one left and one right, and two deep "common source nodes". We first localized the sources using Champagne, MVAB, MCE, and sLORETA and then assessed the connectivity. The inter-

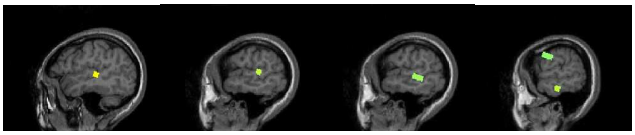

(a)0 to 100ms (b)100 to 200ms (c)200 to 300ms (d)300 to 500ms

Fig. 3. Performance on a language processing task where the subject hears a noun (at 0ms) is asked to come up with an associated verb. The activations shown in (a) through (d) show a flow of activation from superior temporal gyrus ventrally to anterior temporal gyrus and dorsally to a pre-central gyrus (motor) area. This dual stream of activations has been reported in fMRI and is a current model of language processing.

dipole correlations are depicted in the diagram found in Figure 5(a) where the color of the lines between the sources denotes the strength of correlation, with red being high and blue being weak (see colorbar in Figure 5(e). The line type indicates whether the mixing was instantaneous (dashed) or non-instantaneous (solid). The "common source" nodes were added to simulate the effect of instantaneous correlations on the metrics. The voxels in the left and right networks were all instantaneously coupled with the common source voxels, but the coupling was a different strength.

In a second experiment, we increased the coupling between the common-sources and all the voxels relative to the strength of coupling within the networks in order to test the robustness to common-source interference. We also wanted to test the performance of MVAR when we do not have access to the common source time-courses, as is often the case with artifacts and sources of noise. We simulated the data with all seven nodes, but then used the five nodes of the networks of interest to perform the MVAR analysis. We used only the Champagne reconstructions for this analysis.

III. Results and Discussion

Figure 1 through Figure 3 show the results obtained from running Champagne on real brain data. See the captions for a description of the results. The results obtained from Champagne from these data sets agree with conventional activation patterns. The auditory perturbation task is a novel MEG dataset for which commonly used source localization algorithms did not uncover meaningful activity, but Champagne is able to localize correlated activity. Figure 4 show the source reconstruction results from Champagne (a), MCE (b), MVAB (c), and sLORETA (d) respectively. The white and black circles mark the true locations of the sources and the surface plot shows the maximum intensity projection of the power of the source estimate at every voxel, illustrating the inferred location of the sources. While MCE came close to uncovering all 5 nodes of the two networks, Champagne was the only algorithm able to resolve the location and time-courses of the two networks entirely. (Both common source nodes were uncovered with Champagne, but one was below the threshold of the image in Figure 4 (a).)

The functional connectivity results of the first experiment are depicted in Figure 5 and the second experiment are depicted in Figure 6. As described above, in the first experiment we used the coherence measure to reconstruct the

correlations (shown by the color of the lines) and imaginary coherence to determine which correlations are instantaneous or non-instantaneous (shown by dashed versus solid lines). The similarity of the ground-truth (a) and Champagne (b) plots demonstrates that these two quantities can be used in conjunction to uncover the strength and lags (instantaneous vs. non-instantaneous) of interactions in a network of brain areas. The common sources are not shown to confound the connectivity results with Champagne. MCE (c), MVAB (d) and sLORETA (not shown) showed an over-estimation of the connectivity and fail to reconstruct the ground-truth connectivity. We decided to proceed with the connectivity analysis with all the algorithms, regardless of success, because it is common practice to do region-of-interest analyses.

In the second experiment, we increased the coupling of the common-sources to investigate the resilience of the functional connectivity methods to strong common-source component. We found that the pair-wise metrics were not able to uncover the two networks (with any algorithm) due to this increased common-source coupling (not shown). MVAR, on the other hand, is able to uncover the networks by providing accurate information on the direction of the interactions and the time lag of these interactions, Figure 6.

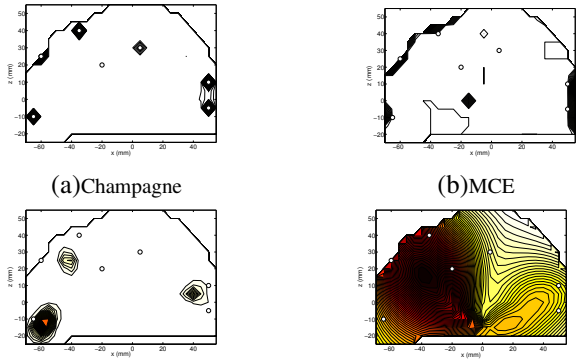

Fig. 4. Source Localization: Source localization results for (a)Champagne, (b) MCE, (c) MVAB, and (d) sLORETA. The circles show the seeded location of the sources and the surface plot shows the estimated location of the sources.

IV. Conclusion

We have demonstrated that Champagne is able to uncover brain activity in both simulated and real data. The sparse solution to the inverse problem obtained from Champagne is well suited for functional connectivity analyses as the number of active voxels is significantly smaller than with other techniques commonly used, such as MVAB and sLORETA. We have demonstrated that in certain situations, MVAR outperforms coherence and IC in uncovering interactions and lags in a network of brain areas in simulation. We plan to extend our functional connectivity techniques to the real brain data presented here. This method holds promise in improving both source localization and functional connectivity analyses in tasks that require the integration of information across a number of brain areas.

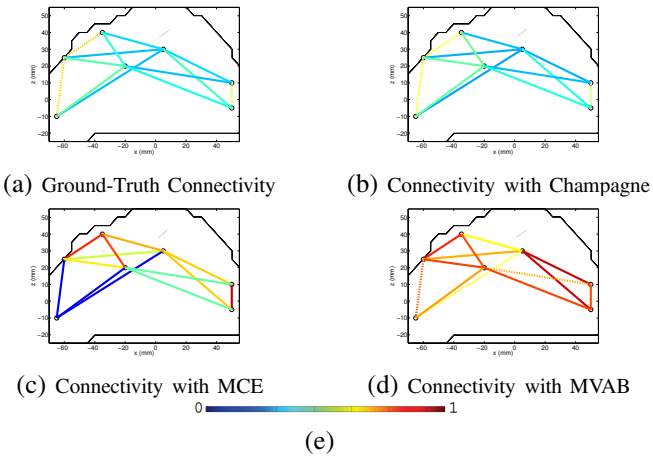

Fig. 5. Functional Connectivity: (a) Ground-truth functional connectivity between sources and "common sources". Reconstructed networks using (b) Champagne, (c) MCE and (d) MVAB. The color (see (e)) shows the strength of coupling and the line type shows the lag of integration.(solid for instantaneous, dashed for non-instantaneous).

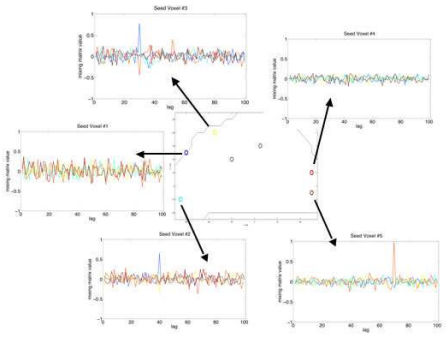

Fig. 6. Functional Connectivity: Plot of the rows of the MVAR mixing matrix obtained for each seed voxel; the time-courss were obtained using Champagne. The reconstructed connectivity found with Champagne is nearly identical to the true connectivity. This plot shows that voxel 1 cause voxels 2 and 3, and that voxels 4 causes voxels 5. The values here are normalized to the maximum.

References

[1] S.S. Nagarajan, et al., "A probabilistic algorithm for robust interference suppression in bioelectromagnetic sensor data," Stat Med. vol. 26, no. 21, pp. 3886–910 Sept. 2007.

[2] G. Nolte, et al. Identifying true brain interaction from EEG data using the imaginary part of coherency," Clinical Neurophysiology. vol. 100, no. 10, pp. 2292-307, 2004.

[3] R.D. Pascual-Marqui, "Standardized low resolution brain electromagnetic tomography (sloreta): Technical details," *Methods and Findings in Experimental and Clinical Pharmacology*, vol. 24, no. Suppl D, pp. 5–12, 2002.

[4] K. Sekihara and S.S. Nagarajan, "Adaptive Spatial Filters for Electromagnetic Brain Imaging," Springer; 1 edition (June 6, 2008).

[5] K. Matsuura, et al., "Selective minimum-norm solution of the biomagnetic inverse problem," *IEEE Trans. Biomed. Eng.* vol. 42, pp. 608-615, 1995.

[6] D. Wipf, et al., "A Unified Bayesian Framework for MEG/EEG Source Imaging," *Neuroimage* vol. 44, no. 3,pp. 947-966, 2009.

[7] D. Wipf, et al., "Estimating the Location and Orientation of Complex, Correlated Neural Activity using MEG," *Advances in Neural Information Processing Systems 21* 2009.

[8] D. Wipf, et al., "Robust Bayesian Estimation of the Location, Orientation, and Timecourse of Multiple Correlated Neural Sources Using MEG," *Neuroimage* In Revision.